Accepted Manuscript

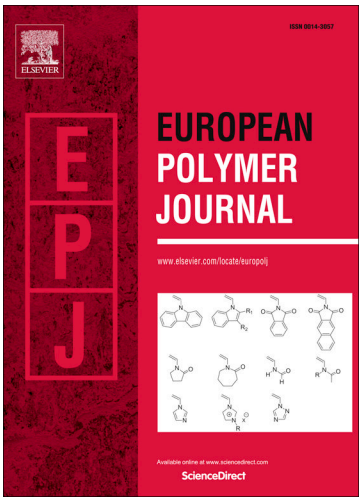

Novel Polycaprolactone /Hydroxyapatite Nanocomposite Fibrous Scaffolds by Direct Melt-Electrospinning Writing

Abdalla Abdal-hay, Naghmeh Abbasi, Marcin Gwiazda, Stephen Hamlet, Saso Ivanovski

PII: S0014-3057(18)30634-7
DOI: https://doi.org/10.1016/j.eurpolymj.2018.05.034
Reference: EPJ 8432

To appear in: *European Polymer Journal*

Received Date: 3 April 2018
Revised Date: 12 May 2018
Accepted Date: 25 May 2018

Please cite this article as: Abdal-hay, A., Abbasi, N., Gwiazda, M., Hamlet, S., Ivanovski, S., Novel Polycaprolactone /Hydroxyapatite Nanocomposite Fibrous Scaffolds by Direct Melt-Electrospinning Writing, *European Polymer Journal* (2018), doi: https://doi.org/10.1016/j.eurpolymj.2018.05.034

Novel Polycaprolactone /Hydroxyapatite Nanocomposite Fibrous Scaffolds by Direct Melt-Electrospinning Writing

Abdalla Abdal-hay[1], Naghmeh Abbasi[2], Marcin Gwiazda[3], Stephen Hamlet[2, 4], Saso Ivanovski[1*]

[1]*The University of Queensland, School of Dentistry, Oral Health Centre Herston, 288 Herston Road, Herston QLD 4006, Australia,*

[2]*School of Dentistry and Oral Health, Griffith University Gold Coast Campus, QLD, Australia,*

[3]*Warsaw University of Technology, Faculty of Material Science and Engineering, 141 Woloska str., 02-507, Warsaw, Poland,*

[4]*Menzies Health Institute, Griffith University, Gold Coast Campus, QLD, Australia.*

*Corresponding Author:

E-mail: s.ivanovski@uq.edu.au (S. Ivanovski)

Tel: +61733658064

Keywords: Melt-electrospinning writing; PCL; Bone Tissue Engineering; Biodegradable Composite Materials; 3D Scaffold

Abstract:

Melt electrospinning writing (MEW) using an automated stage has recently been developed as a direct additive manufacturing method for the fabrication of orderly, precise and complex porous 3D fibrous structures that can promote cell infiltration and growth. The further incorporation of inorganic particles within fibrous scaffolds is desirable in order to enhance bioactivity, however this remains challenging with the MEW fabrication process. To address this challenge, flexible, osteoconductive, medical grade polycaprolactone (m-PCL) - hydroxyapatite (HAp) composite 3D fibrous structures with high porosity (96- 98 %) and fully interconnected pore architectures were fabricated using MEW under precisely controlled parameters. The physical properties of these 3D fibrous composite scaffolds including fibre size, mechanical characteristics, and *in vitro* degradation rate were investigated. The results showed that the composite m-PCL/HAp fibrous scaffolds degraded in an alkaline environment at 37 °C faster than plain m-PCL and provided a favourable platform for the infiltration and growth of human osteoblasts. Moreover, confocal imaging confirmed that the scaffolds contained HAp nano-particles (NPs) which induced a more homogeneous distribution of cells within the scaffold particularly after 7 days of culture. Osteoblast activity and viability in the m-PCL/HAp composite scaffolds indicated a favourable cell/material interaction, suggesting great potential for use in mineralised tissue reconstruction / regeneration applications.

1. Introduction

Recently, there has been significant interest in three dimensional (3D) scaffolds with the ability to mimic the extracellular matrix (ECM) of natural tissue and the capability to promote tissue regeneration by promoting favourable cellular orientation [1-3]. In tissue engineering (TE) applications, the presence of a scaffold is essential as a matrix for subsequent cell colonization, migration, growth, and ECM deposition **[4, 5].** To achieve this, solution electrospinning has been widely employed in many 3D fabrication approaches [6-10]. This approach provides a biomimetic cellular environment which resembles the ECM of native tissue. However, a major issue with solution electrospun meshes is the low pore size associated with random layering of sub-micrometre diameter fibres, which can act as a barrier to cellular infiltration [10-13]. Several studies have attempted to increase the mesh pore size (to ~20 μm) to promote cell invasion, migration and growth [11, 12]. Despite these attempts, both *in vitro* and *in vivo* studies have reported that the minimum pore size required for bone ingrowth into three-dimensional scaffolds needs to be ~100 μm [14-16] which cannot be obtained by solution electrospinning. Furthermore, solution electrospun fibrous mats are usually comprised of randomly oriented fibres [17]. Efforts to organise the deposition of the fibres [13, 18-21] have been hampered by charge accumulation effects on the solution electrospun fibres, which upon attempted ordered fabrication become bound as one coherent structure with limited porosity [22].

Melt electrospinning writing (MEW) has recently emerged as a direct approach for the fabrication of ordered, well-interconnected porous structures with favourable pore size (over 100 μm) suitable for TE applications [19, 22-24]. Although the MEW approach facilitates the fabrication of scaffolds with properties required for cell ingrowth and tissue vascularization, only pristine (plain) thermoplastic fibres have been fabricated using MEW. In most cases, plain polymer scaffolds are not ideal for TE applications due to their bio-inert nature. In the context of bone regeneration, this translates to a lack of osteoinductivity which can delay or even prevent osteogenesis [14].

Calcium phosphate (CaP) is the main inorganic component of vertebrate bone and teeth. Hydroxyapatite (HAp), biphasic calcium phosphate (BCP) and β-tricalcium phosphate (β -TCP) represent typical examples of CaP minerals, which are known to integrate well with surrounding bone tissue and facilitate bone tissue growth [25-29]. Therefore, CaP biomaterials are commonly used in orthopaedic and dental surgery as bone void fillers [30] or as a coating material on polymeric implants to provide enhanced bioactivity [28, 31]. To stimulate osteo-conduction, calcium phosphate mineral coated onto the surface of melt electrospun polycaprolactone (PCL) polymer fibres has been widely utilized with polymeric scaffolds [23, 31-33]. However the CaP layer has low stability due to the weak interfacial bonding between the CaP compounds and the PCL fibre surface. This may result in the CaP layer peeling off upon contact with an aqueous environment, thus diminishing or losing its osteo-conductive capacity (Fig. S1 of supporting information).

It has been suggested that the incorporation of HAp nanocrystals within melt-electrospun fibres may mitigate these disadvantages and biopolymers with HAp additives have indeed been shown to have excellent chemical and biological affinity to bone tissues [34, 35]. Our strategy therefore was to use MEW in order to design a bioactive, flexible scaffold with precise control over filament ordination, thus creating 3D composite structures with highly ordered pores that are sufficiently large (over 100 μm) to encourage cell infiltration and growth. The aim of this study was to design a PCL/HAp composite scaffold that mimics the morphological and microstructural properties of cancellous bone tissue, using a biocompatible material (PCL) which incorporates a HAp biologically active phase able to stimulate osteogenesis. PCL is a semicrystalline thermoplastic polymer with low melt temperature (~ 60 °C), thus enabling the possibility to be easily melt processed [36-38]. This study reports for the first time, the incorporation of synthesized HAp nanoparticles (NPs) into a medical grade polycaprolactone (m-PCL) melted fibres using a direct writing approach to enable the production of 3D structures for bone tissue engineering applications.

2. Experimental

2.1.Synthesis of HAp nanoparticles (HAp NPs)

HAp (Ca_{10} $(PO_4)_6(OH)_2$) nanocrystals were synthesised by a wet chemical precipitation method as previously reported in the literature [39] using 0.6 M $(NH_4)_2HPO_4$ and 1M $Ca(NO_3)_2.4H_2O$ (The Ca/P ratio was 1.67 when these solutions are mixed to produce stoichiometric HAp) at 90 ºC. The fabrication processes are explained in detail in the supplementary materials. The morphological properties and chemical composition of synthesised HAp nanocrystals are also displayed in Fig. S2 of the supporting information.

2.2. Fabrication of composite fibrous scaffold by MEW

The experimental design of the fabrication of the composite fibre scaffold using MEW is summarized in Fig. 1. Medical grade PCL granules (m-PCL, 120 kDa, Corbion, Australia) were dissolved in chloroform at 15 wt. %. HAp powder at 3 and 7 wt. % (based on m-PCL contribution) were added into the m-PCL solution under vigorous stirring at multiple stages to avoid agglomeration. After adding HAp powder, the composite solution was ultrasonically agitated for 20 min then left overnight under vigorous stirring. After homogenization for 30 min in an ultrasonic bath, 50 ml of the m-PCL solution was cast into 125 mm × 20 mm petri dishes and allowed to dry under vacuum for three days. The cast samples were then chopped with a sharp scalpel blade into small pieces before being placed in the plastic syringe barrel of the MEW device. Prior to the spinning process, 2 gm of the material placed within the syringe was heated inside an oven at 80 ºC for 30 min to melt.

The set-up of the MEW has been described in detail in previous publications [22, 40]. Briefly, the MEW device includes a 2 ml plastic syringe with a 21 Gauge needle, a 7 kV high voltage source (DX250R, EMCO, Hallein, Austria), a 20 ml/h feed rate which is controlled by a pneumatically regulated melt feeding system (regulator, FESTO, Berkheim, Germany) and a movable aluminium collector plate triggered by G-code (MACH 3 CNC

software, ARTSOFT, Livermore Falls, USA). The tip-collector distance was 10 mm. The electrical heating system was proportional integral-derivative-regulated (TR400, Delta-t, Bielefeld, Germany) to ensure a stable melt temperature profile. Melted polymer was drawn vertically from the nozzle tip with the electrostatic force generated from the high potential voltage applied between the nozzle and the grounded collector. The spinning parameters, such as applied voltage, flow rate and collector speed, were initially optimized and then precisely controlled to obtain continuous fibres for the various experiments.

2.3. Scaffold Characterization and Cell Culture

The characterization of the prepared plain m-PCL and m-PCL/HAp composite scaffolds, i.e. surface properties, physical, chemical and mechanical properties, degradation in alkaline solution and cell biology are described in detail in the supporting information.

3. Results and Discussion

3.1.Physical structure and Chemical composition of the prepared composite scaffolds

The scaffolds were electrospun using a composite material containing ultrasonically dispersed HAp nanoparticles (NPs) within an m-PCL carrier. The incorporation of bioactive HAp inorganic nanoparticles within the polymer fibres, combined with the large pore size and highly interconnected porosity achieved through the MEW technique, offers clear advantages in terms of cell colonization, vascularization, nutrient and metabolite exchange, cell infiltration and growth. Poly(ϵ-caprolactone) (PCL) was used for the fabrication of the melt electrospun fibres as it possesses a wide melt processing range owing to its low melting point (60 °C) and high thermal stability [24, 41] and has been proven to be an excellent substrate for bone tissue engineering [23] owing to its biocompatibility, biodegradability, and flexibility.

Figure 2 shows typical SEM images, Energy-dispersive X-ray (EDX) spectra and diameter distributions of the as-fabricated plain and composite fibrous scaffolds. The melt

electrospun scaffolds were composed of orderly stacked fibres with a 0-90° pattern (Fig. 2a). The SEM images showed mildly roughened fibres after the incorporation of HAp nanoparticles (Fig. 2b-d). The HAp particles were distributed uniformly on the surface and embedded within the melt electrospun fibres. Moreover, the particles in 3 %HAp appeared to protrude from the fibre surface (Fig. 2c).

EDX coupled with SEM was used to detect CaP in the scaffold. At 3 wt. %, EDX analysis could not detect the CaP spectra in the composite matrix suggesting that the HAp particles were fully encapsulated within the fibre matrix at this concentration. At 7 wt. %, EDX showed small CaP peaks with weak intensity (Fig. 2e). Incorporation of HAp NPs significantly ($p<0.001$) increased the fibre diameter from 10.79±0.34 µm for plain m-PCL to 16.84±2.41 and 20.46±1.09 µm for 3 and 7 wt. % HAp concentrations, respectively (Fig. 2f). This subsequently contributed to a decrease in the pore size from 200 to 190 µm ($p>0.05$).

Apart from the morphology and structure, the overall porosity of the m-PCL/HAp scaffolds was estimated using the following equation [26, 42]:

$$\varepsilon = \left(1-\frac{\rho}{\rho_o}\right)\times 100$$

$$\rho = \frac{m}{V}$$

$$\rho_o = (x+y)/\left(\frac{x}{\rho_{PCL}} + \frac{y}{\rho_{HAp}}\right)$$

where ε is the porosity; ρ is the density of the scaffolds calculated from the volume ($V= \frac{\pi}{4} diameter^2 \times$ h of a circular sheet punched from the prepared composite fibrous scaffold) and dry weight (m) of the scaffold; x: y is the mass ratio of components in the composite; and ρ_o is derived from the standard density of m-PCL (1.145 gcm^{-3}) and HAp (3.157 gcm^{-3}). The calculated overall porosity of plain m-PCL, 3 and 5 % HAp were 98, 97.2 and 96 % respectively which is favourable for cellular infiltration and the diffusion of metabolites, nutrients and waste. Collectively, these findings suggest that the incorporation of

HAp nanoparticles did not show any significant ($p>0.05$) effect on the pore size and porosity properties of the melt electrospun composite fibrous scaffolds.

FTIR analysis of the fabricated scaffolds (Fig. 3a) showed characteristic peaks corresponding to HAp and m-PCL molecules, as previously reported [26, 42]. The intensity (transmittance percentage) of characteristic IR bands of HAp in the composite scaffold are co-related to the loading amount of HAp within the electrospun scaffold, as shown by the bands assigned for PO_4^{3-} (Fig. 3a. inset). As the HAp loading increased the bands intensity also showed an increase. Some IR bands of the m-PCL/HAp composite showed a small shift to a higher wavelength likely due to the formation of chemical bonds between the HAp particles and m-PCL during the fabrication process, as has been reported by Kim et.al [43].

3.2.Thermal analysis

Differential scanning calorimetry (DSC) measurements were performed to examine the thermal behaviour of the fabricated fibrous scaffold before and after incorporation of HAp. The results from the DSC are presented in Fig. 3b and summarized as an inset table. The melting points and the heat of fusion (the melting heat) are indicative of the polymer crystallinity, as described elsewhere [26]. Two independent cycles of heating and cooling runs were performed, in which the first cycle was able to eliminate the polymer heat history. With a reference point of 136 J/g for 100% crystalline m-PCL [44], the degree of crystallinity Xc % of the polymer scaffold was determined. A sharp crystalline melting temperature was observed for m-PCL in both the plain form and as composite scaffolds. The crystalline fraction of m-PCL is reduced to some extent after the incorporation of HAp. Slightly different glass transition temperature (Tg) values were registered on the DSC heating runs which may be caused by the effects of thermal history on the thermal behaviour. The melting temperature following the loading of HAp NPs is almost unchanged compared with that of the plain m-PCL scaffolds. A decrease in the enthalpy of fusion and the Tg suggests that the

crystallinity and perfection of the crystal structure are reduced, proving that the ameliorated thermal stability and the flexibility remains the same after HAp loading [26]. The interactions between m-PCL and HAp NPs (i.e., the hydrogen bonding between them) can be attributed to further deterioration in crystallinity after the addition of HAp NPs into the composite scaffolds.

3.3. Biodegradation behaviour of the fabricated scaffolds

The total weight change of the scaffolds after incubation in an alkaline environment (pH 8.5) for a period of up to 28 days is shown in relation to incubation time in Fig. 4. This pH choice was due to the fact that in healing wounds, the microenvironment is shifted slightly to more alkaline conditions [45]. Hence, the degradability of the membranes was tested in this representative alkaline conditions. The results suggested that in scaffolds incorporating HAp particles, a significant acceleration in degradation rate was observed (Fig. 4a). It should be noted that within 28 days, less than 5% mass loss was observed from m-PCL and a significant ($p<0.01$) increase was measured in the composite scaffolds, as shown in Fig. 4a. Higher HAp concentrations correlated with a higher weight loss. Moreover, the samples containing the higher HAp amount dissolved more quickly, i.e., 7% >3% >plain m-PCL (0 %), suggesting that the HAp dissolved faster than the m-PCL. This increase may be due to the more hydrophilic nature of HAp, as has been previously shown by our group [28, 39, 46], which facilitated the interaction of water with the polymeric fibres, and the hydrolysis and subsequent release of HAp particles from the fibre surface, as depicted in Fig. 4b and c.

3.4. Cellular response

To evaluate the cellular response to the scaffold composition, the constructs were seeded with human osteoblasts and cultured in vitro for 1, 4 and 7 days, with cell numbers evaluated at these time points via DNA content estimation using PicoGreen. Furthermore, metabolic activity was assessed at Day 7 using Alamar blue. To evaluate the cellular

response, all scaffolds (each with a diameter of 5 mm) were seeded with 20,000 cells, which results in ~90% confluence on the surface. An ideal tissue engineered scaffold should promote both good cellular attachment and infiltration, and a balanced combination of both is needed to eventually promote whole tissue formation. Attaining this balance in MEW scaffolds has proven to be achievable. Specifically, the melt-electrospun scaffolds allowed the cells to spread and migrate within the scaffold, with the large pore sizes facilitating substantial cellular infiltration [18, 20]. Both the scaffold material and the respective porous architecture play a major role in cellular performance [42]. Continuous cell growth over time can be observed from the confocal images in Figure 5a. All scaffolds showed good cell attachment and spreading at each time interval, with the highest speeding and bridging seen in the 7 % HAp composite scaffold after seven days. On both the plain and composite m-PCL/HAp scaffolds, cells infiltrated deep into the scaffold (Fig. 5b). From day 1, the osteoblasts had infiltrated into the scaffold to a depth of ~350 μm (Fig. 5b). By day 4, most of the cells had grown up to the perimeter of the scaffolds, as can be seen from the 3-D z-stack object (Fig. 5b). Furthermore, by day 7, cells were present throughout the scaffold and the number of cells had increased considerably. These promising results correlated directly to the more open and larger pore network structure shown in Fig. 5b, which allowed the cells an easier path for deep infiltration and greater cell proliferation.

Next, the cellular response was evaluated quantitatively, and as shown in Fig. 6. All scaffolds were associated with good cell viability with an improvement in growth and proliferation over the incubation time-frame. DNA quantification showed that the composite scaffold had a better cell attachment capacity than plain m-PCL scaffolds, as evidenced by the higher DNA content at the early (Day 1) time point (Fig. 6a). Further, the results of the DNA assay indicate that osteoblasts cultured on m-PCL/HAp composites had a higher proliferation rate at the longer time points (7-day) compared to cells cultured on plain m-PCL

and even tissue culture plate (TCP), as shown in Fig. 6a. The difference in cell response may be due to the composite scaffold having a slightly lower pore size (~190 μm) and porosity (96%) but larger fibre diameter size compared with plain m-PCL scaffold [22].

The cell viability (Alamar Blue) assay results after 7 days of culture (Fig. 6b) support the results of the DNA content quantification results. These results suggest that the presence of HAp within the m-PCL melt electrospun fibres induce a positive effect on cell viability [42]. Since the increase in the viability is a direct measure of living cells [46], the results suggest that cell proliferation is taking place. The higher cell viability of the m-PCL/HAp composite scaffold compared to plain m-PCL scaffold can be attributed to the presence of HAp, which has been shown to increases surface roughness and wettability and provides functionalisation for cell adherence and growth, compared to plain PCL scaffolds which lack biological recognition sites [19, 46]. These results are in accordance with other authors where cell growth and infiltration within scaffolds increased with the combination of large pore size and bioactive ceramics [42]. Cumulatively, these data show that the melt electrospun scaffolds provide an optimal environment for cellular infiltration and the incorporation of HAp NPs provide for more growth than plain polymeric scaffolds.

4. Concluding remarks

This communication study has demonstrated, for the first time, the incorporation of synthesised HAp nanoparticles at 3 and 7 wt. % within m-PCL melt electrospun fibres to create composite scaffolds using MEW. A preparation process that achieves an even distribution of HAp NPs within the m-PCL melt electrospun fibres is a key requirement avoiding blockages of the jet in order to ‘write’ with a continuous composite fibre. The melt electrospun composite scaffold induced higher cell growth and both plain m-PCL and composite fibres showed good cell infiltration into the scaffold. Degradable composite scaffolds, prepared by combining an additive manufacturing technique and high voltage with

precisely controlled parameters represents a viable solution to achieving adequate biomaterial requirements for tissue engineering strategies. This combination of a well-interconnected highly porous structure with large pore size and incorporated bioactive ceramic is suitable for the promotion of osteoblast cell seeding, infiltration and growth, and represents an excellent candidate for bone tissue engineering strategies.

References

[1] S. Battista, D. Guarnieri, C. Borselli, S. Zeppetelli, A. Borzacchiello, L. Mayol, D. Gerbasio, D.R. Keene, L. Ambrosio, P.A. Netti, Biomaterials 26 (2005) 6194-6207.
[2] M.A. Brennan, A. Renaud, A.L. Gamblin, C. D'Arros, S. Nedellec, V. Trichet, P. Layrolle, Biomed Mater 10 (2015) 045019.
[3] M.S. Kim, G. Kim, Carbohydrate Polymers 114 (2014) 213-221.
[4] R. Scaffaro, F. Sutera, F. Lopresti, Materials & Design 131 (2017) 334-342.
[5] R. Scaffaro, A. Maio, F. Lopresti, L. Botta, Polymers 9 (2017) 76.
[6] Y. Yang, S. Basu, D.L. Tomasko, L.J. Lee, S.-T. Yang, Biomaterials 26 (2005) 2585-2594.
[7] S. Yang, K.-F. Leong, Z. Du, C.-K. Chua, Tissue engineering 7 (2001) 679-689.
[8] C. Huang, N.L. Thomas, European Polymer Journal 99 (2018) 464-476.
[9] J. Pal, D. Wu, M. Hakkarainen, R.K. Srivastava, European Polymer Journal 96 (2017) 44-54.
[10] R. Scaffaro, F. Lopresti, L. Botta, European Polymer Journal 96 (2017) 266-277.
[11] Y.M. Ju, J.S. Choi, A. Atala, J.J. Yoo, S.J. Lee, Biomaterials 31 (2010) 4313-4321.
[12] Q.P. Pham, U. Sharma, A.G. Mikos, Biomacromolecules 7 (2006) 2796-2805.
[13] F.A. Sheikh, H.W. Ju, J.M. Lee, B.M. Moon, H.J. Park, O.J. Lee, J.H. Kim, D.K. Kim, C.H. Park, Nanomedicine 11 (2015) 681-691.
[14] M.M.C.G. Silva, L.A. Cyster, J.J.A. Barry, X.B. Yang, R.O.C. Oreffo, D.M. Grant, C.A. Scotchford, S.M. Howdle, K.M. Shakesheff, F.R.A.J. Rose, Biomaterials 27 (2006) 5909-5917.
[15] C.E. Wilson, J.D. de Bruijn, C.A. van Blitterswijk, A.J. Verbout, W.J.A. Dhert, Journal of Biomedical Materials Research Part A 68A (2004) 123-132.
[16] T.C. Lim, K.S. Chian, K.F. Leong, Journal of Biomedical Materials Research Part A 94A (2010) 1303-1311.
[17] D.H. Reneker, A.L. Yarin, H. Fong, S. Koombhongse, Journal of Applied physics 87 (2000) 4531-4547.
[18] D. Zhang, J. Chang, Advanced Materials 19 (2007) 3664-3667.
[19] P.D. Dalton, C. Vaquette, B.L. Farrugia, T.R. Dargaville, T.D. Brown, D.W. Hutmacher, Biomaterials Science 1 (2013) 171-185.
[20] W. Teo, M. Kotaki, X. Mo, S. Ramakrishna, Nanotechnology 16 (2005) 918.
[21] S. Ramakrishna, An introduction to electrospinning and nanofibers, World Scientific, 2005.
[22] T.D. Brown, P.D. Dalton, D.W. Hutmacher, Advanced Materials 23 (2011) 5651-5657.
[23] C. Vaquette, S. Ivanovski, S.M. Hamlet, D.W. Hutmacher, Biomaterials 34 (2013) 5538-5551.
[24] T.D. Brown, F. Edin, N. Detta, A.D. Skelton, D.W. Hutmacher, P.D. Dalton, Materials Science and Engineering: C 45 (2014) 698-708.
[25] A. Abdal-hay, L.D. Tijing, J.K. Lim, Chemical Engineering Journal 215-216 (2013) 57-64.
[26] S. Uma Maheshwari, V.K. Samuel, N. Nagiah, Ceramics International 40 (2014) 8469-8477.
[27] A. Rogina, P. Rico, G. Gallego Ferrer, M. Ivanković, H. Ivanković, European Polymer Journal 68 (2015) 278-287.
[28] A. Abdal-hay, H.R. Pant, J.K. Lim, European Polymer Journal 49 (2013) 1314-1321.

[29] H.J. Lee, S.E. Kim, H.W. Choi, C.W. Kim, K.J. Kim, S.C. Lee, European Polymer Journal 43 (2007) 1602-1608.
[30] J.S. Lee, W.L. Murphy, Advanced Materials 25 (2013) 1173-1179.
[31] A. Abdal-hay, P. Vanegas, A.S. Hamdy, F.B. Engel, J.H. Lim, Chemical Engineering Journal 254 (2014) 612-622.
[32] T. Kokubo, S. Ito, Z.T. Huang, T. Hayashi, S. Sakka, T. Kitsugi, T. Yamamuro, Journal of Biomedical Materials Research 24 (1990) 331-343.
[33] A. Cüneyt Tas, Biomaterials 21 (2000) 1429-1438.
[34] M. Sivakumar, K. Panduranga Rao, Biomaterials 23 (2002) 3175-3181.
[35] F. Zhao, Y. Yin, W.W. Lu, J.C. Leong, W. Zhang, J. Zhang, M. Zhang, K. Yao, Biomaterials 23 (2002) 3227-3234.
[36] R. Scaffaro, F. Lopresti, L. Botta, S. Rigogliuso, G. Ghersi, Journal of the Mechanical Behavior of Biomedical Materials 63 (2016) 303-313.
[37] R. Scaffaro, F. Lopresti, L. Botta, A. Maio, Composites Part B: Engineering 98 (2016) 70-77.
[38] R. Scaffaro, F. Lopresti, L. Botta, S. Rigogliuso, G. Ghersi, Macromolecular Materials and Engineering 301 (2016) 182-190.
[39] A. Abdal-hay, N.A. Barakat, J.K. Lim, Ceramics International 39 (2013) 183-195.
[40] T.D. Brown, F. Edin, N. Detta, A.D. Skelton, D.W. Hutmacher, P.D. Dalton, Materials Science and Engineering: C 45 (2014) 698-708.
[41] M.D. Edwards, G.R. Mitchell, S.D. Mohan, R.H. Olley, European Polymer Journal 46 (2010) 1175-1183.
[42] A.H. Ambre, D.R. Katti, K.S. Katti, Journal of Biomedical Materials Research Part A 103 (2015) 2077-2101.
[43] H.-W. Kim, J.C. Knowles, H.-E. Kim, Biomaterials 25 (2004) 1279-1287.
[44] R. Scaffaro, F. Lopresti, A. Maio, L. Botta, S. Rigogliuso, G. Ghersi, Composites Part A: Applied Science and Manufacturing 92 (2017) 97-107.
[45] A. Nasajpour, S. Ansari, C. Rinoldi, A.S. Rad, T. Aghaloo, S.R. Shin, Y.K. Mishra, R. Adelung, W. Swieszkowski, N. Annabi, Advanced Functional Materials 28 (2018).
[46] A. Abdal-hay, F.A. Sheikh, J.K. Lim, Colloids Surf B Biointerfaces 102 (2013) 635-643.

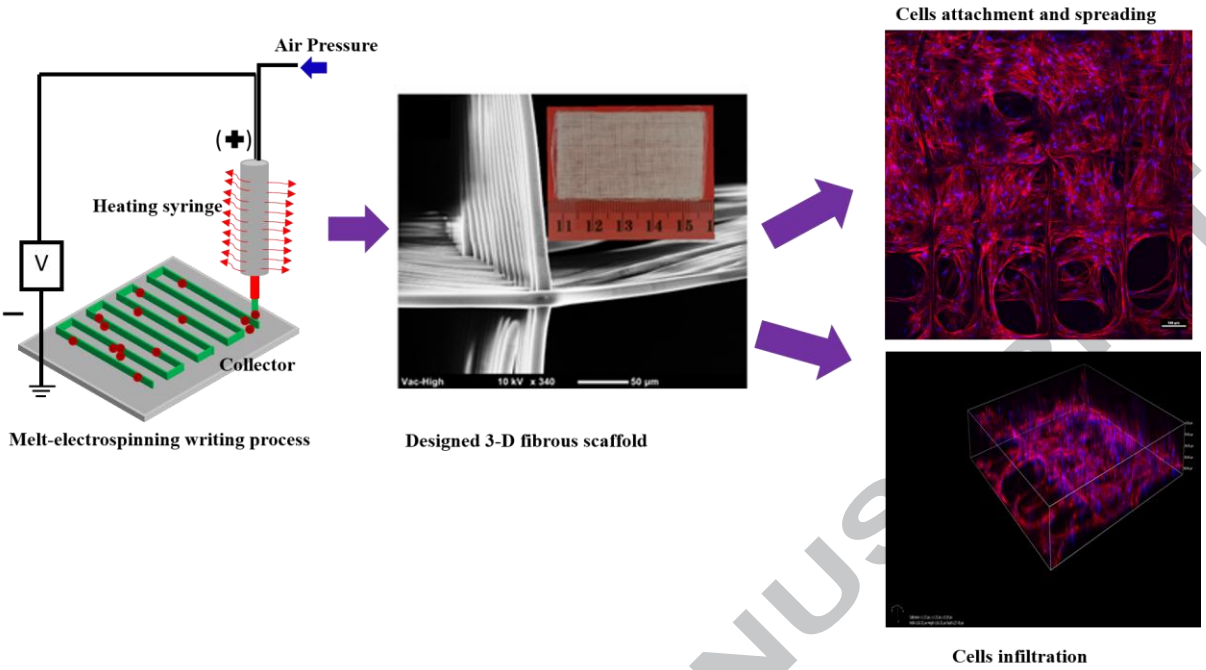

Figures and captions

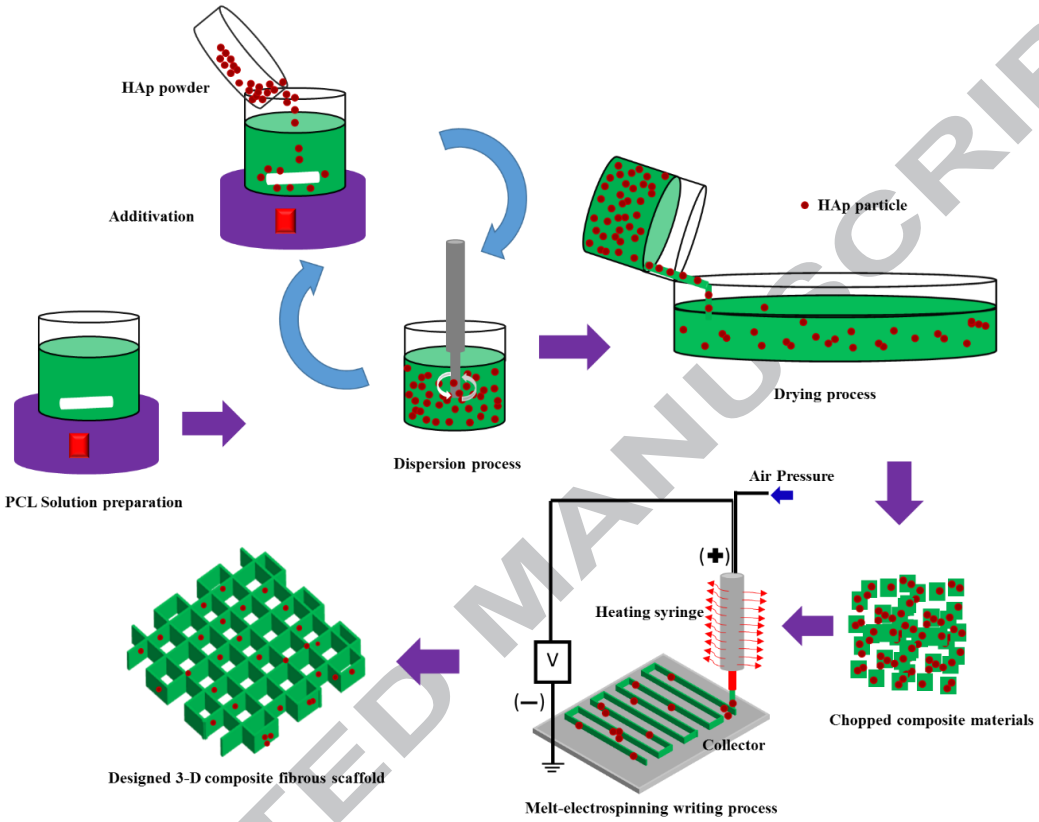

Fig. 1: Illustrates a schematic diagram of the 3D fibrous composite scaffolds fabricated by the melt electrospinning writing process.

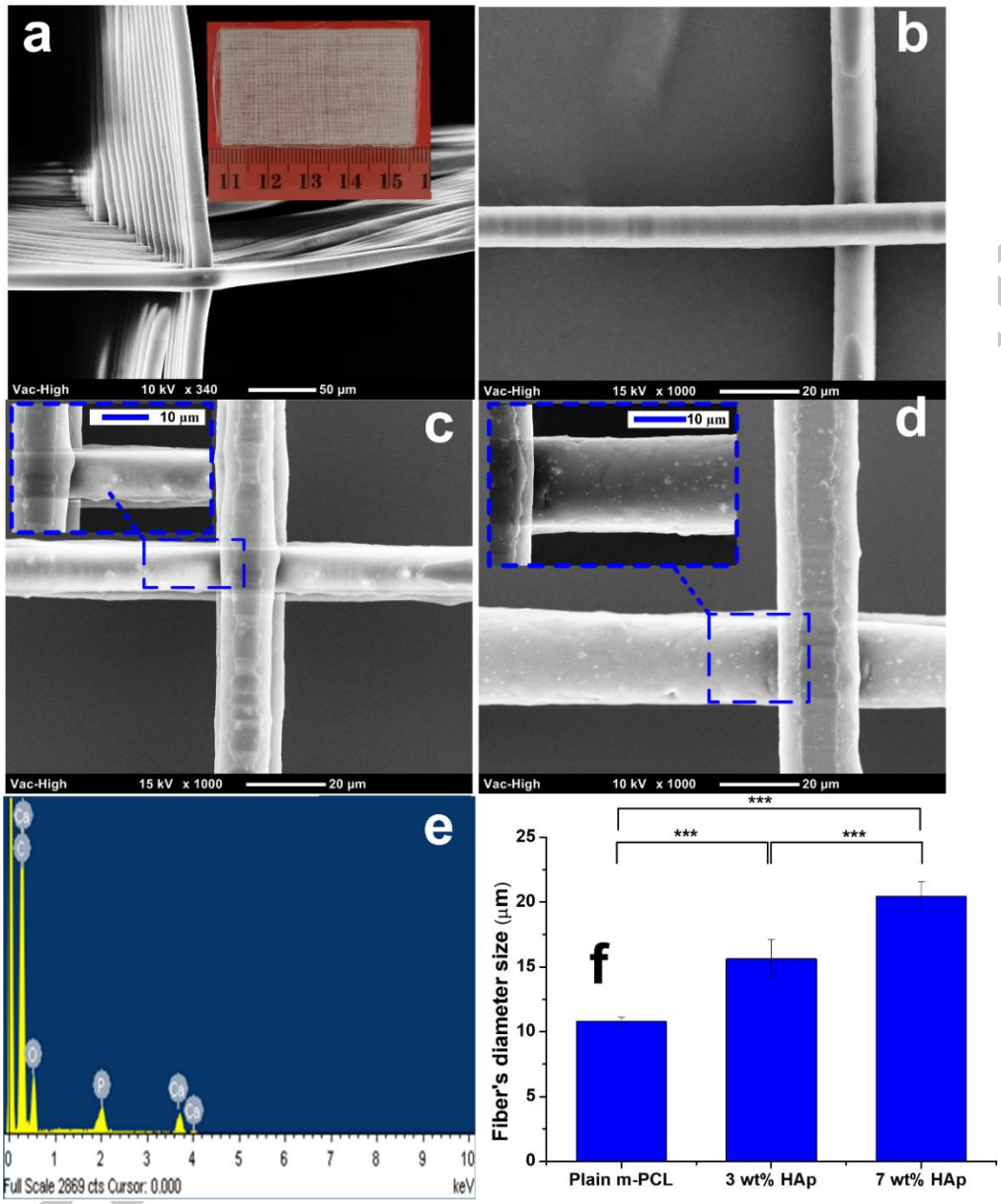

Fig. 2: Shows SEM images of electrospun fibers fabricated by the melt electrospinning writing (MEW) approach (a) low magnification image of the fabricated scaffold with orderly stacked fibers and well-interconnected pores; (b) plain m-PCL; (c) 3 wt% HAp; (d) 7 wt% HAp; (e) EDS profiles of 7 wt% HAp composite scaffold and (f) fiber diameter measurements in the fabricated scaffolds. The plain electrospun fibers had a significantly smaller diameter compared with the composite scaffold fibers. Bars show significant differences in the diameter between plain and composite scaffolds. Inset of panels 2c and 2d show a higher magnification image of the composite fibers. ***shows statistical significance $p < 0.001$

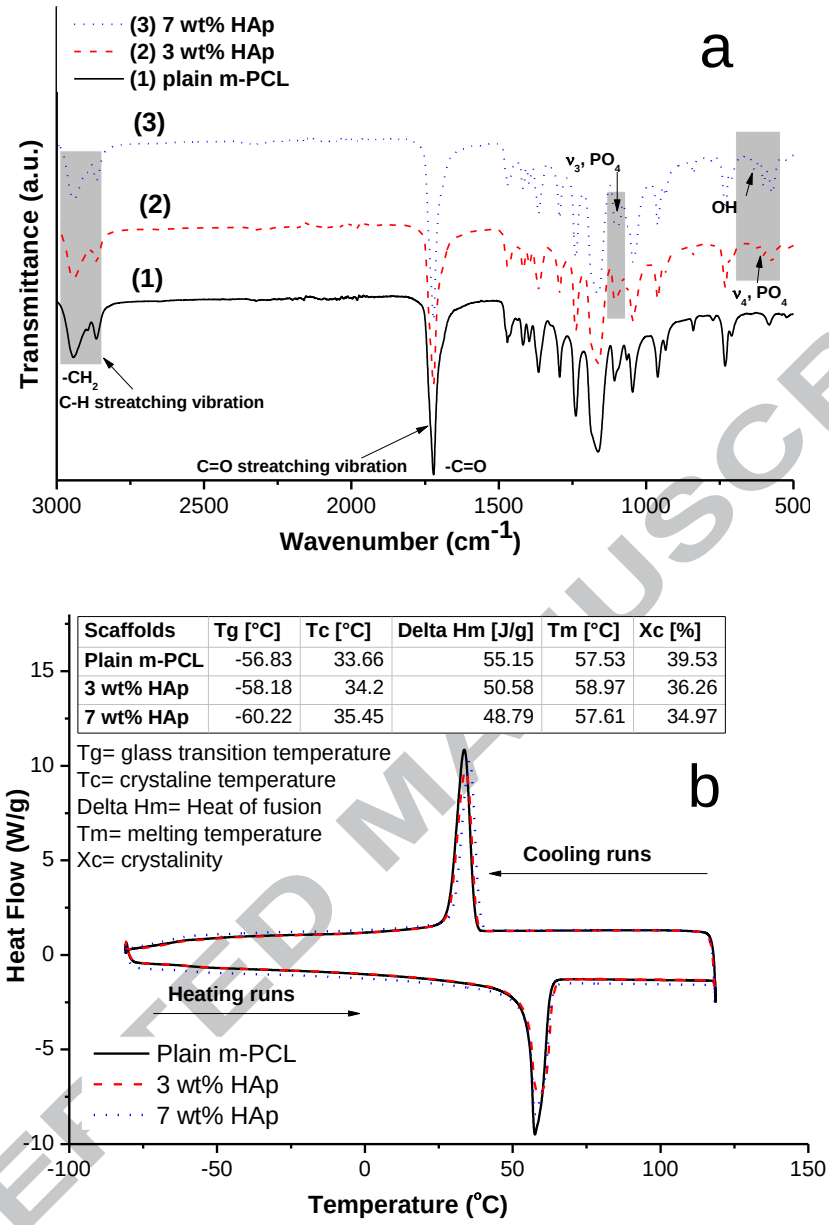

Scaffolds	Tg [°C]	Tc [°C]	Delta Hm [J/g]	Tm [°C]	Xc [%]
Plain m-PCL	-56.83	33.66	55.15	57.53	39.53
3 wt% HAp	-58.18	34.2	50.58	58.97	36.26
7 wt% HAp	-60.22	35.45	48.79	57.61	34.97

Fig. 3 (a) FTIR spectra and (b) DSC curves of plain and composite scaffolds fabricated by the MEW approach. Both FTIR spectra exhibit sharp peaks for PO_4^{3-}: 1042 cm^{-1} (v_3) and 605and 563 cm^{-1} (v_4) which are characteristics bands for HAp. The FTIR analysis showed typical transmittance characteristics bands for HAp and these results confirm that the synthesized HAp NPs are loaded into the m-PCL matrix. The thermal properties of the as-fabricated composite fibrous scaffolds are summarised in a table inset of (b). The thermal properties, such as, Tg, Tm and delta Hm, were identified from the second heating runs, while the Tc was determined from the cooling scan.

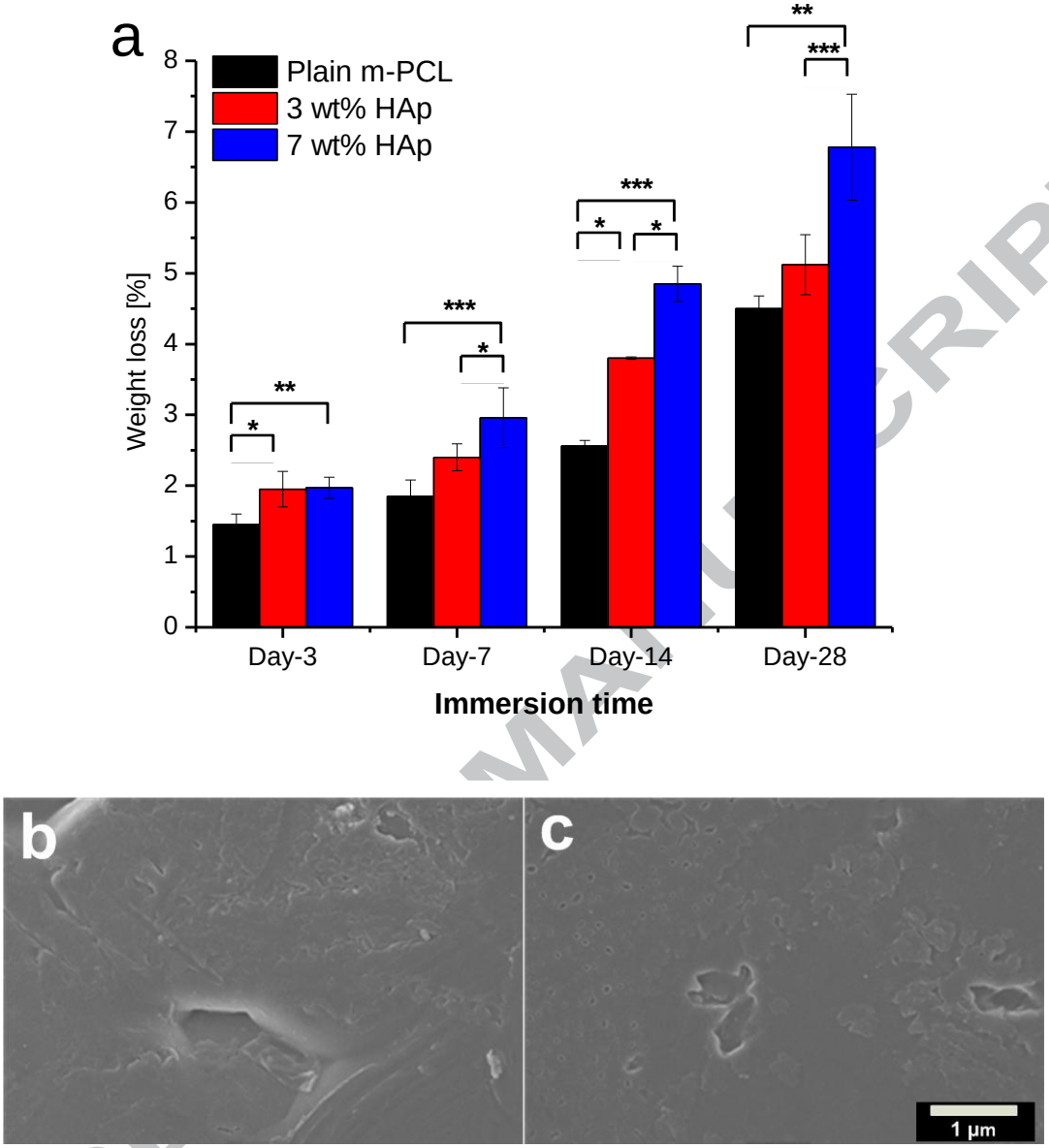

Fig. 4 (a) Percent weight loss over 28 days of immersion in an aqueous alkaline environment. (b) Surface morphology of plain m-PCL and (c) 7 wt.% HAp composite scaffolds after 28 days. *depicts statistical significance at $p < 0.05$, **$p < 0.01$ and ***$p < 0.001$

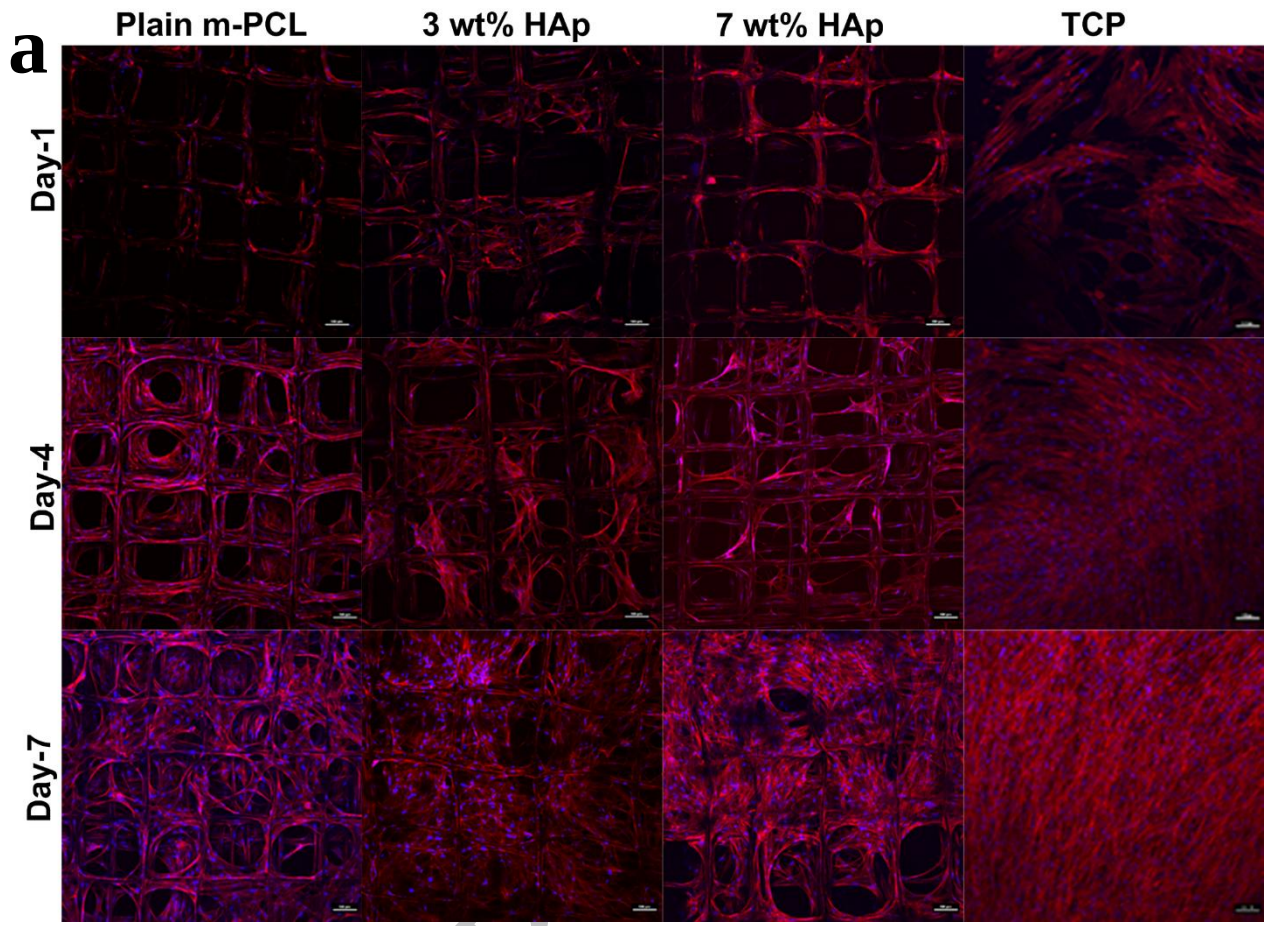

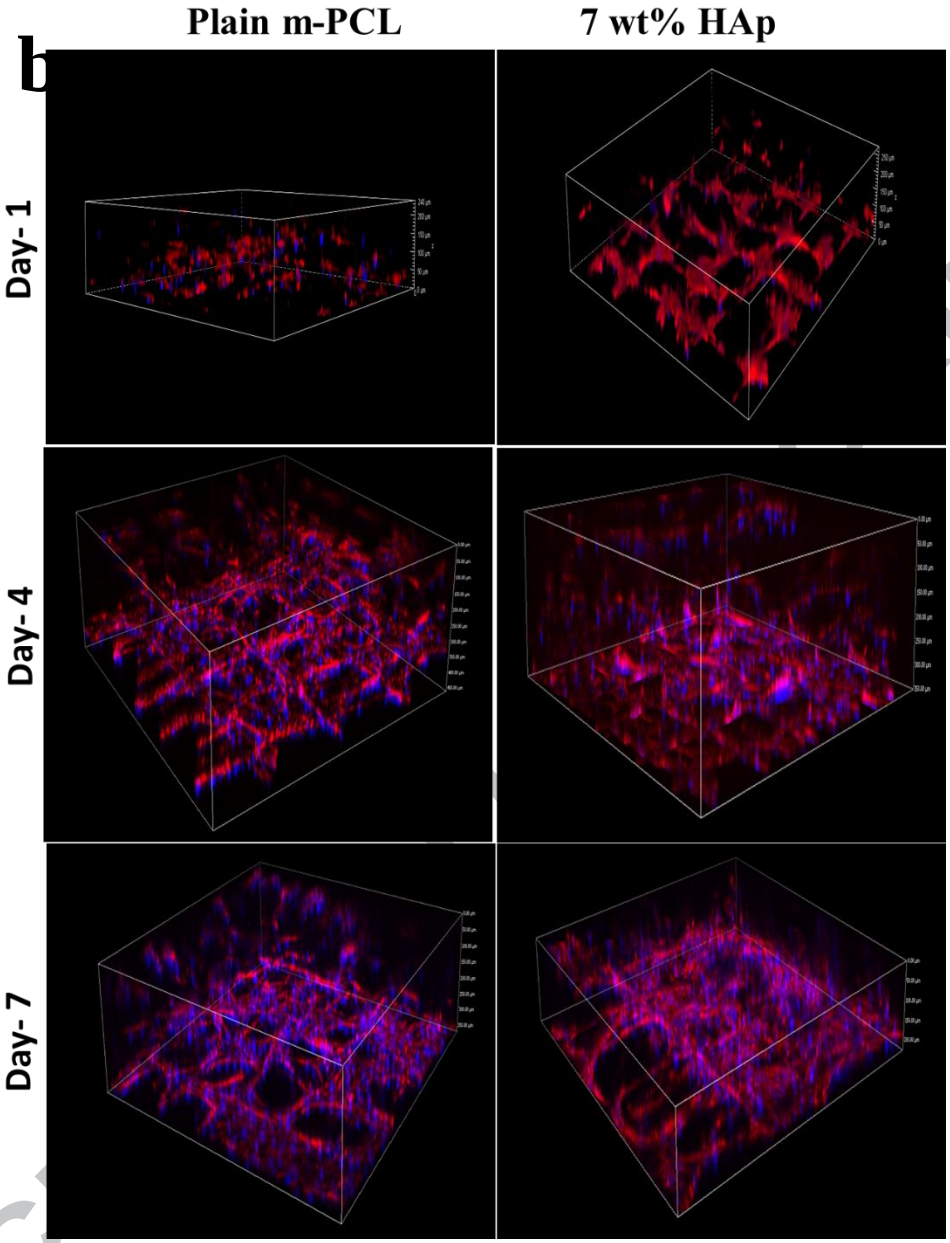

Fig. 5 Laser confocal microscopy images of human osteoblasts cells cultured on plain m-PCL and m-PCL/Hap composite scaffolds fabricated by the MEW approach. (a) cell morpoglogy and cell spreading over 7 days culture (scale bar = 100 µm). (b) 3-D object z-stacking showing infiltation, spread and growth of cells at different time intervals. Each stack corresponds to 1 µm in the *z*-direction of the scaffold (scale bar = 350 µm). The samples were stained with phalloidin conjugated with Alexa Fluor 632 fluorescent dye to target F-actin (Red). Cell nuclei (blue) were visualized by staining with fluorescent 4',6-diamidino-2-phenylindole (DAPI).

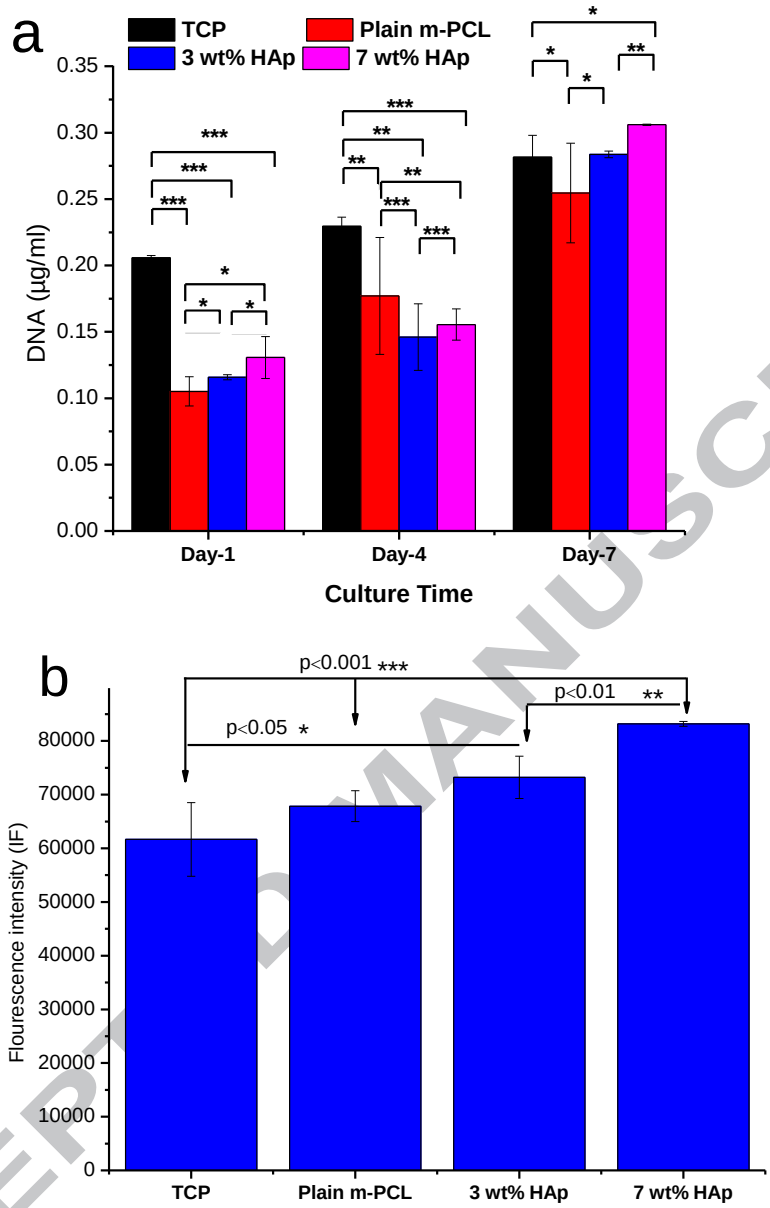

Fig. 6. (a) Human osteoblast cells adhesion and (b) proliferation on plain m-PCL and m-PCL/HAp composite melt electrospun fibrous scaffolds as a function of culture time were quantified by DNA estimation (PicoGreen assay) and cell activity (Alamar Blue assay) respectively. The amount of DNA gradually increased with culture time and showed the highest DNA content was on composite scaffolds loaded with 7 wt% HAp NPs after 7 days culture. Cell activity also was highest on 7 wt% HAp scaffolds at 7 days culture compared to plain m-PCL and tissue culture plastic (TCP). Asterisks show statistically significant differences (*$p < 0.05$, **$p < 0.01$, ***$p < 0.001$, two-way ANOVA followed by post-hoc Tukey test).